Available online at www.sciencedirect.com
SCIENCE DIRECT®
Nuclear Instruments and Methods in Physics Research A 544 (2005) 458–464
NUCLEAR INSTRUMENTS & METHODS IN PHYSICS RESEARCH Section A
www.elsevier.com/locate/nima

Chaotic particle trajectories in high-intensity finite-length charge bunches

Stuart R. Hudson*, Hong Qin, Ronald C. Davidson

Princeton Plasma Physics Laboratory, PO Box 451, Princeton NJ 08543, USA

Available online 7 march 2005

Abstract

A Vlasov–Maxwell equilibrium for a charged particle bunch is given in the beam frame by the distribution function that is a function of the single-particle Hamiltonian $f = f(H)$, where in an axisymmetric cylinder $H = \mathbf{p}^2/2m + \kappa_\perp r^2/2 + \kappa_z z^2/2 + q\phi(r,z)$, the kinetic energy is $\mathbf{p}^2/2m$, $\kappa_\perp$ and κ_z are the external focusing coefficients in the transverse and longitudinal directions, and ϕ is the electrostatic potential determined self-consistently from Poisson's equation $\nabla^2\phi = -4\pi q \int \mathrm{d}^3 p f(H)$. The self-field potential ϕ introduces a coupling between the otherwise independent r and z motions. Under quite general conditions, this leads to chaotic particle motion. Poisson's equation is solved using a spectral method in z and a finite-difference method in r, and a Picard iteration method is used to determine ϕ self-consistently. For the thermal equilibrium distribution $f = A\exp(-H/T)$, the single-particle trajectories display chaotic behavior. The properties of the chaotic trajectories are characterized.

PACS: 52.25.G

Keywords: Chaotic motion; Lyapunov exponent; Tangent map

1. Introduction

It has been noted that charged particle beams in thermal equilibrium will possess particles that follow chaotic trajectories and the existence of chaotic particles may lead to a degradation of the beam quality [1]. It is thus important to study and understand the conditions that lead to chaotic behavior. This article examines such trajectories in finite-length charge bunches. The commonly used Lyapunov exponent [2,3] quantifies how sensitive a trajectory is to initial conditions, a defining characteristic of chaos. Particular attention is given to resonant motion and the stability of periodic trajectories is examined. Periodic trajectories play an important role, as chaotic trajectories arise near unstable periodic orbits.

We have not yet formulated a comprehensive description of the extent of chaos in phase space as

*Corresponding author.
E-mail address: shudson@pppl.gov (S.R. Hudson).

0168-9002/$ - see front matter © 2005 Elsevier B.V. All rights reserved.
doi:10.1016/j.nima.2005.01.278

a function of the system parameters, although some general observations are interspersed throughout the text. The numerical approach that is presented here may enable an efficient and insightful description of the onset and extent of chaotic particle motion in charge bunches with self-consistent electric potential.

2. Thermal equilibrium

We begin with the Hamiltonian for a single particle, of charge q, confined by an external focusing potential of the form $V_{\rm ext} = \kappa_\perp r^2/2 + \kappa_z z^2/2$, where $\kappa_\perp$ and κ_z are the external focusing coefficients in the transverse, r, and longitudinal, z, directions. A charged particle will also feel the effect of the electrostatic potential, $\phi(r,z)$, generated by the charge bunch itself. The full Hamiltonian for a single particle in the beam frame is then

$$\mathscr{H} = \frac{p_r^2}{2m} + \frac{p_\theta^2}{2mr^2} + \frac{p_z^2}{2m} + \frac{\kappa_\perp r^2}{2} + \frac{\kappa_z z^2}{2} + q\phi \qquad (1)$$

where p_r, p_θ and p_z are the momenta canonical to r, θ and z, respectively, and are given by $p_r = m\dot{r}$, $p_\theta = mr^2\dot{\theta}$ and $p_z = m\dot{z}$, where the 'dot' denotes the time derivative.

To describe the charge bunch it is convenient to specify an equilibrium distribution function, $f(\mathbf{x},\mathbf{p})$, where $\mathbf{x}$ and $\mathbf{p}$ are the position and momentum coordinates in phase space. The number density $n(\mathbf{x})$ of particles is given by $n = \int f\,\mathrm{d}^3p$. Any distribution function that is a function solely of the single particle Hamiltonian represents a Vlasov–Maxwell equilibrium [4]. A particularly appropriate form of the distribution function, which we choose for illustration, is that which describes a charge bunch in thermal equilibrium

$$f(H) = \frac{n_0}{(2\pi mT)^{3/2}} \exp(-\mathscr{H}/T). \qquad (2)$$

By expressing the self-generated electric field $\mathbf{E} = -\nabla\phi$, and absorbing Eqs. (1) and (2) into Poisson's equation, $\nabla\cdot\mathbf{E} = 4\pi qn$, we obtain

$$\nabla^2\phi = -4\pi qn \qquad (3)$$

with number density $n = n_0 \exp(\kappa_\perp r^2/2 + \kappa_z z^2/2 + q\phi)$. In general, ϕ must be determined numerically. By introducing the normalized lengths $\bar{r} = r/r_{\rm b}$ and $\bar{z} = z/r_{\rm b}$, where $r_{\rm b}$ is defined $r_{\rm b} = \sqrt{T/\kappa_\perp}$, the normalized potential, $\bar{\phi} = q\phi/T$, satisfies

$$\bar{\nabla}^2\bar{\phi} = -2s_{\rm b}\exp(-\bar{r}^2/2 - \eta\bar{z}^2/2 - \bar{\phi}) \qquad (4)$$

where the physical system is now described by two dimensionless parameters η and $s_{\rm b}$, these being the frequency ratio between the longitudinal and perpendicular motions, $\eta = \kappa_z/\kappa_\perp$, and the ratio of plasma frequency to the perpendicular oscillation frequency, $s_{\rm b} = (4\pi q^2 n_0/m)/2\omega_\perp^2$ where $\omega_\perp^2 = \kappa_\perp/m$. The normalized Hamiltonian, $\bar{\mathscr{H}} = \mathscr{H}/T$, is

$$\bar{\mathscr{H}} = \frac{\bar{p}_r^2}{2} + \frac{\bar{p}_\theta^2}{2\bar{r}^2} + \frac{\bar{p}_z^2}{2} + \frac{\bar{r}^2}{2} + \eta\frac{\bar{z}^2}{2} + \bar{\phi} \qquad (5)$$

where $\bar{p}_r = \bar{r}'$, $\bar{p}_\theta = \bar{r}^2\theta'$, $\bar{p}_z = \bar{z}'$, and prime denotes derivative with respect to the normalized time, $\bar{t} = t\omega_\perp$. Hereafter, we will use the normalized equations: the 'bars' will be dropped and the 'dot' will denote the derivative with respect to the normalized time.

A self-consistent solution to Eq. (3) is constructed numerically. A finite difference method is used in the transverse direction and the even symmetry in the z coordinate allows an even spectral representation for the longitudinal direction $\phi(r,z) = \sum \phi_n(r)\cos(nkz)$, where $\phi_n(r)$ interpolates $\phi_{n,i}$ given on the radial grid. In the results below, 100 radial zones are used between the axis, $r = 0$, and the radial wall, $r = R_{\rm w}$, with normalized $R_{\rm w} = 20$. The periodicity length, L_z, is chosen to ensure the self-field potential at this point is negligible with normalized $L_z = 20$, and 50 Fourier harmonics are used. In cylindrical coordinates, the Laplacian operator takes the form $\nabla^2 = \partial_r^2 + r^{-1}\partial_r + \partial_z^2$. The radial derivatives are approximated by the first-order expressions, with the boundary conditions $\partial_r\varphi(0,z) = 0$ and $\varphi(R_{\rm w},z) =$ const. The structure of the ∇^2 operator becomes a tri-diagonal matrix for each harmonic, which is easily inverted. This allows a Picard iterative solution for the potential: given the spectral representation of the number density, the potential

ϕ is solved; the number density is then determined given the potential. The iterations are terminated when ϕ is no longer changing.

For each selection of the dimensionless parameters (η, s_b), a point in phase space is described by $(r, \theta, z, p_r, p_\theta, p_z)$. The azimuthal angle θ is ignorable, thus the angular momentum p_θ is a constant of the motion. Each particle's trajectory will lie on a constant energy surface. A phase space subset is then specified by (p_θ, H), and a point in this space is given by (r, z, p_r). Note that given (p_θ, H) and (r, z, p_r), p_z is then constrained by Eq. (5). To visualize the structure of phase space, a Poincaré section, $z = 0$ with $p_z > 0$, is chosen. From a given starting point (r, p_r) on this plane, we integrate the equations of motion and plot successive intersections with the Poincaré section. In this manner, we determine if the motion is regular or chaotic. If, in addition to p_θ and H, there exists an invariant of the motion, successive intersections will lie on a curve and the motion is deemed regular. Conversely, if successive intersections tend to fill an area, we may conclude that no additional invariant exists and the motion is stochastic.

Regular and chaotic trajectories are interspersed in phase space. Regular motion lies on invariant surfaces where the frequency ratio is irrational. Resonance zones, or islands, will emerge where the frequency ratio between the r and z motions is rational. Associated with each island chain, are the stable and unstable orbits, which appear as O and X points on the Poincaré plot. Chaotic trajectories arise near the unstable X point. If the islands are so large that they overlap with nearby islands, then regions of extended chaos will be produced.

3. Low-intensity beams

For the case that the self-field potential is zero, the r and z motions are independent and the dynamics is integrable. The 'action' coordinates are determined by $j = \oint p\,\mathrm{d}q/2\pi$ [5], which gives

$$j_r = (\alpha - p_\theta)/2, \tag{6}$$

$$j_z = (z^2\eta^{1/2} + p_z^2/\eta^{1/2})/2 \tag{7}$$

where $\alpha = p_r^2/2 + p_\theta^2/2r^2 + r^2/2$, with corresponding 'angle' coordinates

$$\theta_r = \cos^{-1}[(r^2 - \alpha)/\beta] \tag{8}$$

$$\theta_z = \tan^{-1}(\eta^{1/2} z/p_z) \tag{9}$$

where $\beta = \sqrt{\alpha^2 - p_\theta^2}$. For this case, the use of these coordinates reduces the motion to trivial trajectories as the Hamiltonian takes the form $H = 2j_r + p_\theta + \eta^{1/2} j_z$. The frequency ratio between the transverse and longitudinal oscillations for this case is $\omega_r/\omega_z = 2/\eta^{1/2}$, and a resonance will exist when $2/\eta^{1/2} = p/q$, where p, q are integers. The existence of resonances plays a crucial role in the formation of chaotic trajectories.

For the general case, with non-zero electrostatic potential ϕ, the Hamiltonian takes the form

$$H = 2j_r + p_\theta + \eta^{1/2} j_z + \varphi \tag{10}$$

where $\varphi(\theta_r, \theta_z, j_r, j_z) = \phi(r(\theta_r, j_r), z(\theta_z, j_z))$. When φ is small, perturbative methods may be employed [6]. Writing $H = h_0 + \varepsilon h_1$, where $h_0 = 2j_r + p_\theta + \eta^{1/2} j_z$ and $h_1 = \varphi$, action-angle coordinates (equivalently, invariants of the motion) for the perturbed motion through second order in ε have been constructed and compared to the exact trajectories, as determined by integration of Eqs. (11)–(13) below, as shown in Fig. 1. For sufficiently small self-field potential, the agreement is generally good.

For small perturbations from integrability, the KAM [7–9] theorem (see also Refs. [3,10]) allows expectation that the majority of surfaces will remain intact. In particular, surfaces with sufficiently irrational frequency ratio will survive sufficiently small perturbations. In this case, the perturbative construction of invariants is likely to be fruitful.

However, the frequency ratio is modified by increasing self-field potential, and resonances between the r and z motion will be encountered. As the strength of self-field intensity increases, chaotic regions associated with the unstable periodic trajectories will increase and devour regions of regular trajectories. Perturbation theory will fail in this case, because the invariants no longer exist.

The remainder of this article will illustrate the structure of the phase space and present some

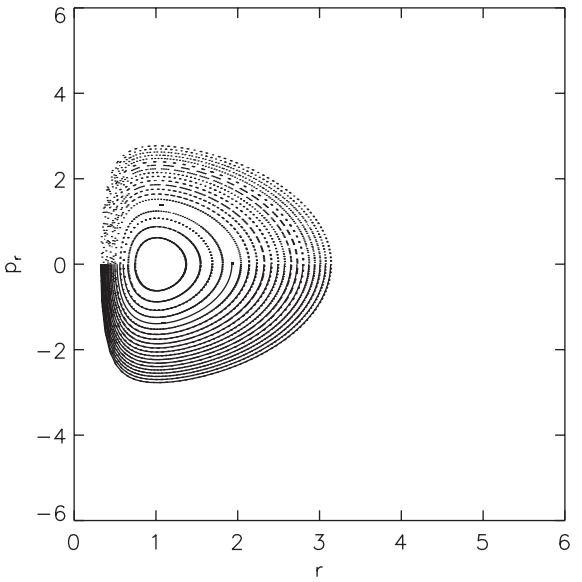

Fig. 1. Comparison of trajectories on Poincaré section with invariant surfaces constructed from second-order perturbation theory for system parameters $(\eta, s_b) = (0.3, 0.1)$ in the phase space subset $(p_\theta, H) = (1.0, H = 5.0)$.

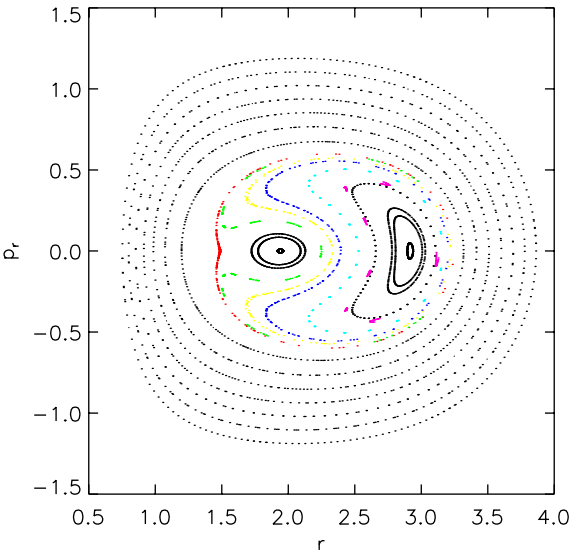

Fig. 2. Poincaré plot for system with $(\eta, s_b) = (0.385, 1.17)$ in the phase space subset $(p_\theta, H) = (1.0, 1.0)$.

theoretical and numerical tools which may be employed to study the chaotic trajectories in high-intensity charge bunches.

4. High-intensity beams

For large values of s_b, we resort to direct numerical integration of the differential equations of motion to determine the single-particle trajectories. With the selection of the plane $z = 0$ as the Poincaré section, it is convenient to consider the independent integration parameter to be θ_z, rather than the time. The equations to be integrated then become

$$\theta_r' = \dot{\theta}_r/\dot{\theta}_z \tag{11}$$

$$j_r' = d_t j_r/\dot{\theta}_z \tag{12}$$

$$j_z' = d_t j_z/\dot{\theta}_z \tag{13}$$

where the $'$ denotes the derivative with respect to θ_z, $\dot{\theta}_r = 2 + \partial\varphi/\partial j_r$, $\dot{\theta}_z = \eta^{1/2} + \partial\varphi/\partial j_z$, $d_t j_r = -\partial\varphi/\partial\theta_r$, and $d_t j_z = -\partial\varphi/\partial\theta_z$. The mapping from the Poincaré section to itself, the Poincaré map, is now obtained by integrating these equations from $\theta_z = 0$ to $\theta_z = 2\pi$. Shown in Fig. 2 is a Poincaré plot showing the emergence of an island chain and a small region of chaos for the system parameters $(\eta, s_b) = (0.385, 1.17)$ and the phase space subset $(p_\theta, H) = (1.0, 1.0)$. Typically, we find that the region of chaotic trajectories is greater as H increases, but we have taken the opportunity here to demonstrate that chaotic trajectories can exist at $H = 1$.

A defining feature of chaos is that particle trajectories have an extreme sensitivity to the initial conditions. To quantify this sensitivity, consider a particle trajectory with initial conditions $\boldsymbol{x}(0) = (\theta_r(0), j_r(0), j_z(0))$ (where, given H, j_z is constrained) and a nearby trajectory $\boldsymbol{x}(0) + \boldsymbol{\delta x}(0)$, where δj_z is constrained to lie in the constant-energy tangent space

$$\delta j_z = -(\partial_{\theta_r}\varphi\delta\theta_r + (2 + \partial_{j_r}\varphi)\delta j_r)/(\eta^{1/2} + \partial_{j_z}\varphi). \tag{14}$$

The trajectories will evolve under Eqs. (11)–(13), and the rate at which the separation $\boldsymbol{\delta x}(\theta_z)$ evolves is characterized by the Lyapunov

exponent σ

$$\sigma(\boldsymbol{x},\delta\boldsymbol{x}) = \lim_{|\delta\boldsymbol{x}(0)|\to 0}\lim_{\theta_z\to\infty}\frac{1}{\theta_z}\ln\frac{|\delta\boldsymbol{x}(\theta_z)|}{|\delta\boldsymbol{x}(0)|}. \tag{15}$$

The limit $|\delta\boldsymbol{x}(0)| \to 0$ is most conveniently treated by linearizing Eqs. (11)–(13) to obtain $\mathrm{d}\delta\boldsymbol{x}/\mathrm{d}\theta_z = \mathbf{T}\delta\boldsymbol{x}$, where $\mathbf{T}$ is the tangent map given by

$$\mathbf{T} = \begin{pmatrix} \frac{\partial\theta_r'}{\partial\theta_r}, & \frac{\partial\theta_r'}{\partial j_r}, & \frac{\partial\theta_r'}{\partial j_z} \\ \frac{\partial j_r'}{\partial\theta_r}, & \frac{\partial j_r'}{\partial j_r}, & \frac{\partial j_r'}{\partial j_z} \\ \frac{\partial j_z'}{\partial\theta_r}, & \frac{\partial j_z'}{\partial j_r}, & \frac{\partial j_z'}{\partial j_z} \end{pmatrix}. \tag{16}$$

Formally, σ depends on the initial $\delta\boldsymbol{x}$, but as the component of $\delta\boldsymbol{x}$ along the most unstable direction will grow most rapidly, this component will dominate the computation. In practice, for an arbitrary initial $\delta\boldsymbol{x}$, the largest Lyapunov exponent will be calculated. After linearizing the equations, all that remains is to follow the trajectory, while evolving the tangent vector, to determine the quantity $\ln|\delta\boldsymbol{x}|/\theta_z$ as $\theta_z \to \infty$ where $|\delta\boldsymbol{x}(0)| = 1$. Typically, a trajectory must be followed hundreds of oscillations for this limit to converge.

For the case of periodic orbits, a tremendous reduction in the computation of the Lyapunov exponent is enabled. A periodic orbit, of type (p,q), satisfies $\theta_r(2\pi q) = \theta_r(0) + 2\pi p$ and $j_r(2\pi q) = j_r(0)$. The full period tangent map, M, at the periodic orbit is obtained by integrating

$$\frac{\mathrm{d}M}{\mathrm{d}\theta_z} = TM \tag{17}$$

one full-period distance $2\pi q$ with initial condition $M = I$, where I is the 3×3 identity matrix. By incorporating the energy conserving constraint Eq. (14), the full period tangent map reduces to a 2×2 matrix.

Important information is contained in this matrix. If the eigenvalues of this matrix are real, the periodic orbit is unstable and the Lyapunov exponent σ_{pq} for the periodic orbit is

$$\sigma_{pq} = \ln\lambda/2\pi q \tag{18}$$

where λ is the eigenvalue. The exponent σ_{pq} may be determined exactly by integrating over the much shorter distance of $2\pi q$. Note that periodic orbits, even unstable periodic orbits, are quite simple to find. As a result of the underlying symmetry of the system, which results in the up–down symmetry of the Poincaré plots, periodic orbits are guaranteed to lie on the symmetry lines $\theta_z = 0, \pi$. The search for periodic orbits becomes a one-dimensional search in j_r along this line.

The Lyapunov exponents for chaotic trajectories arising at the unstable periodic orbits, as calculated from Eq. (15) and shown in color, are compared to the value obtained from Eq. (18), shown as the dotted lines, in Fig. 3. Initially, the Lyapunov exponents from these two methods agree perfectly. To obtain perfect agreement it is necessary to initialize Eq. (15) with a tangent vector that lies in the unstable direction, which is provided by the maximum eigenvalue's corresponding eigenvector. After sufficiently many iterations of the Poincaré map (exactly how many is determined by the accuracy of the integration),

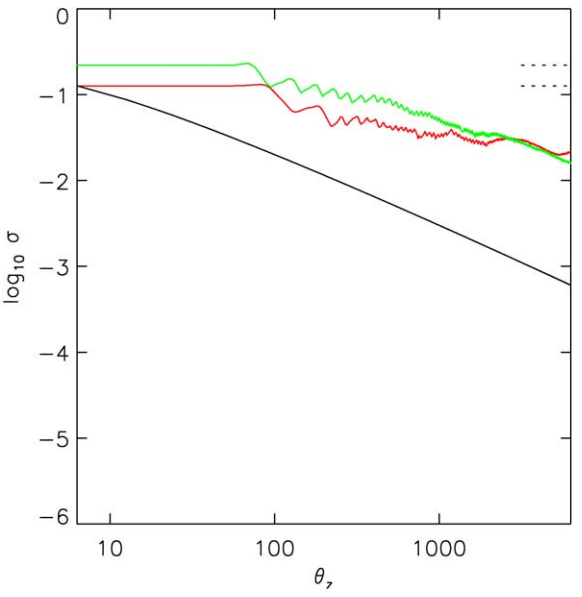

Fig. 3. Lyapunov exponents for chaotic trajectories for a system with parameters $(\eta, s_b) = (0.15, 1.05)$, $(p_\theta, H) = (1.0, 4.0)$. The trajectories are initialized near the $(4,1)$ and $(6,1)$ periodic orbits.

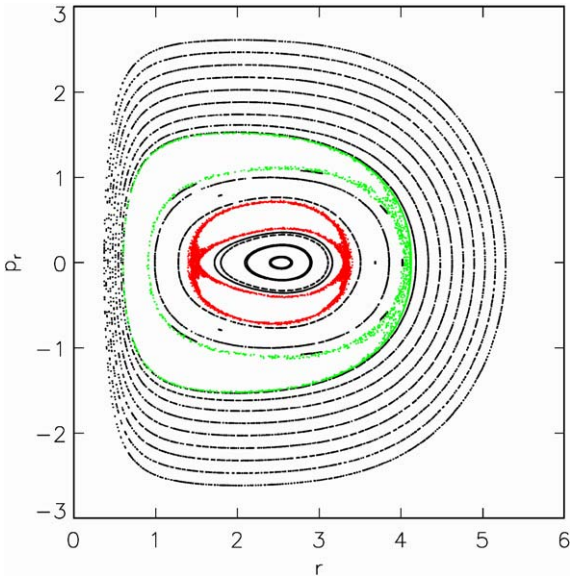

Fig. 4. Poincaré plot for a system with parameters consistent with Fig. 3. The chaotic trajectories are colored as in Fig. 3.

numerical errors accumulate and the trajectory deviates from the true periodic orbit. After this point, the Lyapunov exponent deviates and eventually will converge to a slightly lower value. For reference, the calculation of Eq. (15) for a linearly diverging tangent vector is shown as the decreasing black line. The corresponding Poincaré plot for this case is shown in Fig. 4.

5. Conclusion

Analytical and numerical studies have been presented which enable an efficient characterization of particle trajectories in finite-length charge bunches. In particular a method to quickly determine the Lyapunov exponent of the unstable periodic orbit has been presented. For illustration, a charge bunch in thermal equilibrium has been considered and shown to display chaotic trajectories.

The eigenvalues of the full-period tangent map are related to a quantity called the residue introduced by Greene [11]. The limiting residue of an appropriate sequence of periodic orbits may be used to determine the existence, or non-existence, of an irrational (KAM) surface. Also, the tangent map at the periodic orbits can also be used to estimate island widths [12]. This suggests that a numerically efficient method to quantify the degree of chaos would be to locate several periodic orbits (usually those with the lowest values of q are most important, and conveniently these are of the shortest length), estimate the widths of the islands associated with these periodic orbits and apply a Chirikov style island overlap criterion [13]. Finally, note that the parabolic potential of the applied focusing potential is an approximation. Additional resonances may also exist due to the periodic nature of an applied quadrupole focusing field.

Finally, to assure radial and axial confinement of the charge bunch, the normalized intensity parameter $s_b = \omega_p^2/2\omega_\perp^2$ is restricted to values satisfying $s_b < 1 + \eta/2$, where $\eta = \omega_z^2/\omega_\perp^2$ [4]. Here, $s_b \ll 1$ corresponds to a low-intensity charge bunch, whereas $s_b \to 1 + \eta/2$ corresponds to a low-emittance, space-charge-dominated charge bunch. While we have not yet completed a thorough classification of the chaotic regions of phase space in terms of beam intensity, it should be noted that the system parameters in Fig. 1. correspond to a low-intensity beam, whereas the system parameters in Figs. 2–4 correspond to moderate-to-high beam intensities. Evidently, from the results presented here, the existence of chaotic particle trajectories in a finite-length charge bunch is quite ubiquitous.

Acknowledgements

We thank Ed Startsev for assistance with Eq. (6) and Igor Kaganovich and Neil Pomphrey for useful discussions. This work was supported by the US Department of Energy.

References

[1] C.L. Bohn, I.V. Sideris, Phys. Rev. AT Accel. Beams 6 (2003) 034203.
[2] G. Benettin, L. Galgani, J.-M. Strelcyn, Phys. Rev. A 14 (1976) 2338.
[3] A.J. Lichtenberg, M.A. Lieberman, Regular and Chaotic Dynamics, second ed., Springer, New York, 1992.

[4] R.C. Davidson, H. Qin, Physics of Intense Charged particle beams in high energy accelerators, World Scientific, Singapore, 2001.
[5] H. Goldstein, Classical Mechanics, second ed., Addison-Wesley, MA, 1980.
[6] J.R. Cary, Phys. Rep. 79 (1981) 129.
[7] A.N. Kolmogorov, Dokl. Akad. Nauk. SSR 98 (1954) 469.
[8] V.I. Arnold, Russ. Math. Surv. 18 (1963) 9.
[9] J. Moser, Nachr. Akad. Wiss. Göttingen, Math. Phys. K 1 (1962) 1.
[10] D.K. Arrowsmith, C.M. Place, An introduction to Dynamical Systems, Cambridge University Press, Cambridge, UK, 1991.
[11] J.M. Greene, J. Math. Phys. 20 (1979) 1183.
[12] J.R. Cary, J.D. Hanson, Phys. Fluids B 3 (1991) 1006.
[13] B. Chirikov, Phys. Rep. 52 (1979) 263.